Cell characterization using a protein-functionalized pore†

Andrea Carbonaro,[a] Swomitra K. Mohanty,[a] Haiyan Huang,[b] Lucy A. Godley[c] and Lydia L. Sohn*[a]

Received 4th February 2008, Accepted 26th June 2008
First published as an Advance Article on the web 25th July 2008
DOI: 10.1039/b801929k

We demonstrate a highly-sensitive and label-free method for characterizing cells based on cell-surface receptors. The method involves measuring a current pulse generated when an individual cell passes through an artificial pore. When the pore is functionalized with proteins, specific interactions between a cell-surface marker and the functionalized proteins retard the cell, thus leading to an increased pulse duration that indicates the presence of that specific biomarker. For proof-of-principle, we successfully screened murine erythroleukemia cells based on their CD34 surface marker in both a single and mixed population of cells. Further, we developed a unified constrained statistical model for estimating the ratios of cells in a mixed population. Finally, we demonstrated our ability to screen a small number of cells (hundreds or less) with high accuracy and sensitivity. Overall, our pore-based method is broadly applicable and, in the future, could provide a full range of *in vitro* cell-based assays.

Introduction

Cell characterization through identification of membrane components is an essential element in cell biology,[1,2] disease diagnosis and monitoring,[3,4] and drug discovery.[5] Although current methods for cell analysis, such as flow cytometry,[6] fluorescence microscopy,[7] magnetic-bead column selection,[8] cell-affinity chromatography,[9] and impedance spectroscopy,[10] play an invaluable role in both research laboratories and clinical settings, they do present limitations. For example, traditional approaches often require advanced preparation, including exogenous labeling of cells. Such labeling leads to added incubation time, additional costs, and the possibility of modifying cell physiology and function. As another example, data analysis can be challenging when the available number of cells to be screened is on the order of just a few hundred or less. Finally, traditional approaches do not lend themselves to portability, which can be desirable in certain clinical situations. Given these limitations and constraints, there is still a clear need for new, or at the very least, complementary methods for cell characterization.

Here, we demonstrate a highly-sensitive, accurate, and label-free method for characterizing individual cells based on their cell-surface receptors. Our method employs resistive-pulse sensing (RPS)[11–13] and on-chip artificial pores through which we flow individual cells. RPS is an electronic-sensing technique in which the transient increase, or pulse, in the pore's electrical resistance caused by a particle partially blocking the flow of current through that pore, is detected and recorded. Pulse magnitude corresponds to particle size; pulse width, to the time needed for the particle to pass through the pore; and pulse shape, to how the particle transited through the pore. In our method, the pore is functionalized with proteins and specific interactions between a cell-surface marker and those proteins retard the cell passing through the pore. This correspondingly leads to an increase in the pulse width, thereby indicating the presence of that specific biomarker. While there have been a number of microfluidic devices recently developed for cell-biomarker screening,[14,15] most require fluorescent tagging and/or microscopy techniques for detection. These are in contrast to our pore method, which is label-free and all electronic. We demonstrate the power of our method by screening murine erythroleukemia cells based on their CD34 cell-surface marker in both a single and mixed population of cells. Further, we describe a unified constrained statistical model we have developed for estimating the ratios of cells in a mixed population. Finally, we demonstrate our ability to screen a small number of cells with high accuracy and sensitivity. Our method is broadly applicable and, in the future, could provide a full range of *in vitro* cell-based assays, including the complete phenotypic characterization of specific cells or cell lines.

Materials and methods

Device fabrication

Fig. 1a shows a picture of our device: a polydimethylsiloxane (PDMS) mold sealed to a glass substrate. The PDMS mold is cast from a master[16] and consists of sets of reservoirs and filters and a pore whose diameter is comparable to that of the cells to be interrogated and whose length is typically several hundred microns (see ESI†). The glass substrate has platinum (Pt) electrodes that are lithographically defined prior to PDMS sealing. As well, the region between the electrodes is coated with amino-silane

[a]*Dept. of Mechanical Engineering, University of California at Berkeley, 5118 Etcheverry Hall, Mail Stop 1740, Berkeley, CA, 94720-1740, USA. E-mail: sohn@me.berkeley.edu; Fax: 510-643-5599; Tel: 510-642-5434*
[b]*Dept. of Statistics, University of California, Berkeley, CA, 94720-3860, USA*
[c]*Section of Hematology/Oncology, Dept. of Medicine, The University of Chicago, IL, 60637, USA*

† Electronic supplementary information (ESI) available: Additional Materials and methods section, Fig. S1–S5, Tables S1–S3 and additional references. See DOI: 10.1039/b801929k

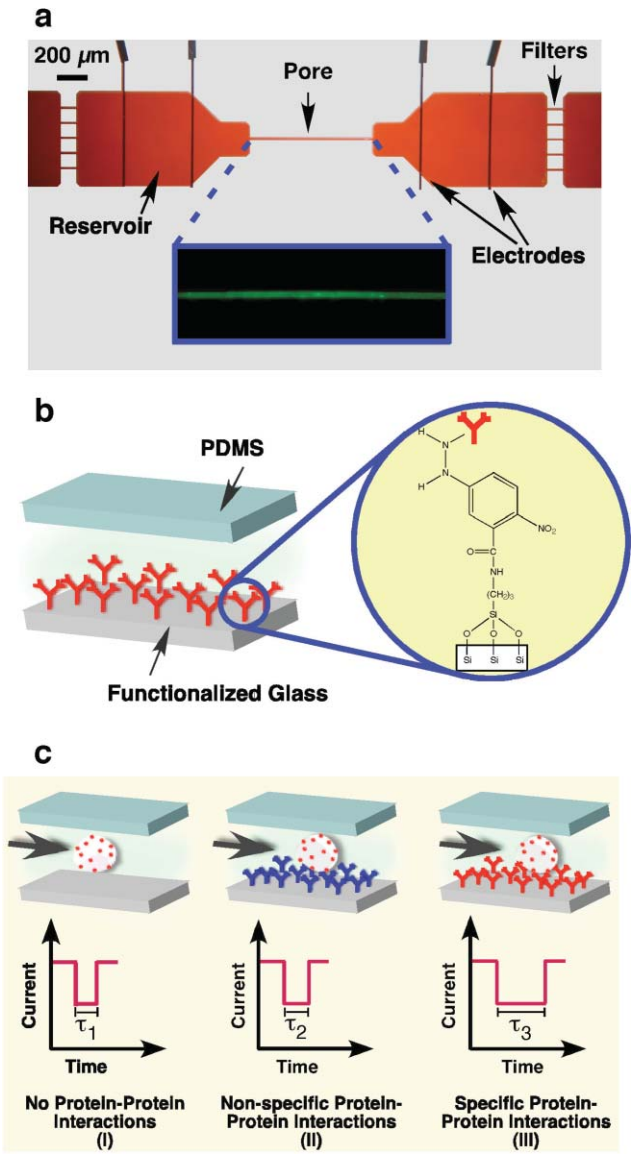

Fig. 1 Device layout and experimental approach. (a) Optical image of one of our pore devices, consisting of 30 μm-deep reservoirs connected by a 15 μm × 15 μm × 800 μm pore. The reservoirs and pore are embedded in a PDMS slab that is sealed to a glass substrate. Filters, of the same cross-sectional area as the pore, are embedded in the PDMS and prevent the pore from clogging. A non-pulsatile pressure drives cells through the pore, and a four-point technique, where the inner (outer) electrodes control the voltage (current), measures the electrical current across the pore. Inset: Epifluorescent image of a pore functionalized with 1500 μg mL^{-1} of FITC-conjugated anti-CD34 antibody. (b) Schematic of the functionalized pore in which a cross-linker (ANB-NOS) covalently binds the protein (red) to the glass substrate. (c) As each cell passes through the pore, a current pulse is detected (I-III). The magnitude reflects cell size and the width indicates cell transit time, τ. A cell travels fastest (τ_1) through an unfunctionalized or "blank" pore (I). Interactions between a specific cell-surface marker and a functionalized pore retard the cell: $\tau_2 \geq \tau_1$ for non-specific interactions (II) and $\tau_3 >> \tau_1$ for specific interactions (III).

groups that are subsequently coupled to a hetero-bifunctional cross-linker, *N*-5-Azido-2-nitrobenzoyloxysuccinimide (ANB-NOS).[17,18] Use of this flexible cross-linker ensures that the functionalized proteins extend beyond the substrate surface (Fig. 1b).[19] After the PDMS slab is oxygen-plasma treated and thermally bonded to the glass substrate, a protein solution (5–1500 μg mL^{-1}) is injected into, and incubated in, the sealed device. UV light is used to activate the ANB-NOS aryl-azide group and subsequently bind the protein covalently to the substrate. Antibodies functionalized *via* this procedure may have reduced activity; however, previous work[20,21] has shown that they are still able to interact specifically with protein receptors. Fig. 1a (inset) is an epifluorescent image of a pore functionalized with 1500 μg mL^{-1} of FITC-conjugated anti-CD34 antibody. In depth details on device fabrication and pore functionalization are provided in the ESI†.

To detect CD34 receptors on the surface of cells, we employ (1) a pore that remains unfunctionalized or "blank"; (2) a pore functionalized with rat IgG2a, an isotype control antibody (eBioscience); and (3) a pore functionalized with anti-CD34 monoclonal antibody (clone: RAM34; isotype IgG2a, k) (eBioscience).

Estimate of the density of functionalized antibody

Following Cozens-Roberts *et al.*[21] who investigated the kinetics of receptor-mediated cell adhesion to a ligand-coated surface, we estimate the functionalized-antibody density, N_{Ab}, within our pores as,

$$N_{Ab} = 0.7[Ab]V_P\left(\frac{A_v}{A_P M_w}\right) \quad (1)$$

Here, [Ab] is the antibody concentration used to incubate the pore, V_p is the pore volume, A_v is Avogadro's number, A_p is the area of the functionalized glass, and M_w is the molecular weight of the antibody. Like Cozens-Roberts *et al.*[21] and Clausen,[22] we assume that only 70% of the antibodies bind to the surface. Thus, for the pores described here, the estimated functionalized-antibody densities are $N_{Ab} \sim 2.6 \times 10^2$ Ab μm^{-2}, when using an antibody concentration of [Ab] = 5 μg mL^{-1}, and $N_{Ab} \sim 7.8 \times 10^4$ Ab μm^{-2}, when using a saturating (see Results and discussion section and Fig. 2e) antibody concentration of [Ab] = 1500 μg mL^{-1}. If only steric limits in a single layer of antibodies [~80 nm^2 antibody^{-1}][23] were to be considered, then the upper limit to the functionalized antibody density would be ~1.2×10^4 antibodies μm^{-2}. The quantitative discrepancy between the antibody density derived from eqn (1) using [Ab] = 1500 μg mL^{-1} and that from steric considerations is due to the aforementioned assumption that 70% of the antibodies bind to the surface. This assumption is highly dependent on the particular functionalization protocol, its efficiency, and substrate type, to name only a few. Nonetheless, we do have agreement regarding the order of magnitude of antibody concentration, *i.e.* ~10^4 Ab μm^{-2}.

Device measurement

Upon device completion, a sample of cells (~10^5 cells mL^{-1}) is injected into one of the outer reservoirs and driven through the filters (which exclude cellular debris and clumps), the inner reservoir, and finally through the pore using a non-pulsatile pressure (typically 10.5 kPa, although pressures as low as

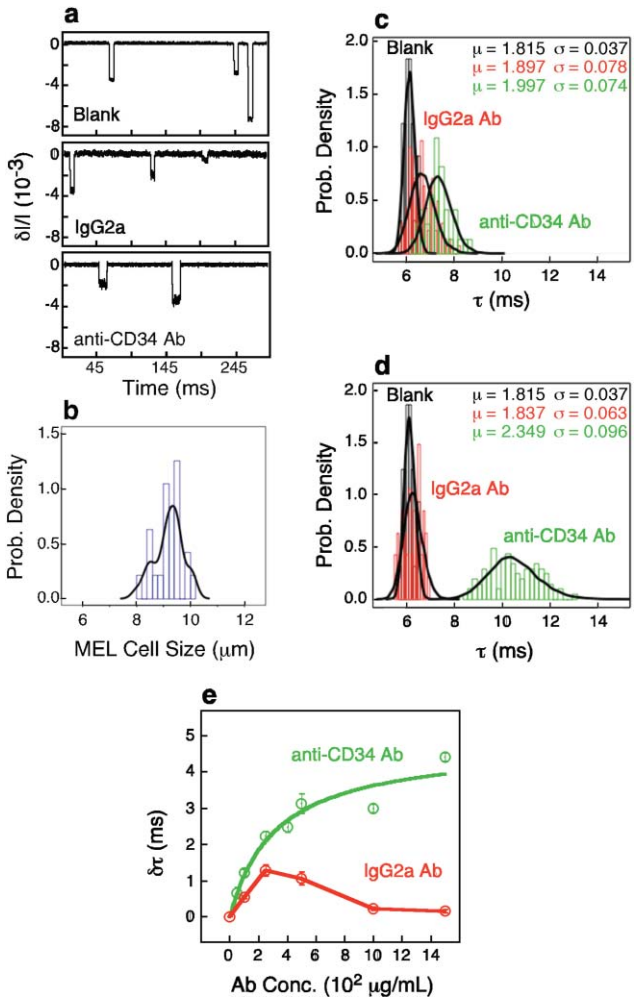

Fig. 2 Detection of CD34 receptors on murine erythroleukemia (MEL) cells. (a) A typical measurement of the normalized current across a blank pore (top), one functionalized with IgG2a antibody (middle), and one functionalized with anti-CD34 antibody (bottom), as MEL cells ($\sim 3 \times 10^5$ cells mL^{-1}) flow (10.5 kPa) one by one. Each downward pulse corresponds to a single cell transiting the pore. (b) Distribution of cell size obtained by analyzing the magnitudes of the resistive-pulses obtained when MEL cells flowed across a blank pore (66 cells). (c) and (d) τ-distributions of MEL cells flowing through a blank pore and a pore functionalized with either IgG2a or anti-CD34 antibody. A log-normal distribution was fitted to each set of data (μ = mean and σ = standard deviation of the distribution calculated after taking the logarithm of the data). In (c), the antibody concentration used was 100 μg mL^{-1}. The number of cells measured was 66 cells in the blank pore, 139 cells in the IgG2a pore, and 37 cells in the anti-CD34 pore. In (d), the antibody concentration was 1500 μg mL^{-1}. The number of cells measured was 48 cells in the IgG2a pore and 103 cells in the anti-CD34 pore. (e) $\delta\tau = (\tau_{avg} - \tau_{avg}^*)$ *vs.* antibody concentration, where τ_{avg} and τ_{avg}^* are average cell transit times for a functionalized pore and blank pore, respectively. Saturation is only observed with increasing anti-CD34 antibody concentrations. Error bars in the figure correspond to $\sigma/\sqrt{\#\text{events}}$, where σ is the standard deviation of the measured τ-distribution.

10.0 kPa and as high as 34.0 kPa have been used). As each cell enters the pore, it partially blocks the flow of current, leading to a transient increase, or pulse, in the pore's electrical resistance (Fig. 1c). A four-point measurement of the current is performed using the Pt electrodes and a constant applied DC voltage (0.2–0.4 V).[11,23,24] As will be discussed in the Results and discussion section, the recorded transit times are on the millisecond time scale for the employed pressure and pore length. Further, sampling for data acquisition is performed at 50 kHz, thus ensuring a sufficient time resolution of 20 μs in all our measurements. All data are recorded and analyzed using custom-written software.

The resistive-pulse magnitude ($\delta I/I$) is directly related to both the volume ratio of cell to pore, V_{cell}/V_{pore}[11–13,23–25] and the cell's orientation with respect to the pore's central axis:[26,27]

$$\frac{\delta I}{I} = \left[f_\perp + (f_\parallel - f_\perp)\cos^2\alpha\right]\frac{V_{cell}}{V_{pore}} \quad (2)$$

Here, $f_\perp$ and $f_\parallel$ are the shape factor's perpendicular and parallel components, respectively, and α is the angle between the electric field $\vec{E}$ and the cell's axis of revolution. Eqn (2) provides a direct and accurate determination of cell size (See ESI for a more in-depth discussion†).

In contrast to the resistive-pulse magnitude, the resistive-pulse *width* indicates the transit time, τ, of a cell passing through a pore (Fig. 1c). A cell's transit time through a functionalized pore (τ_2 or τ_3) is greater than that through an unfunctionalized or "blank" pore (τ_1), due to interactions between the cell-surface marker of interest and the functionalized proteins. If the interactions are non-specific, then $\tau_2 \geq \tau_1$ (II in Fig. 1c). If the interactions are specific, then $\tau_3 >> \tau_1$ (III in Fig 1c).

Cell culture

MEL cells were grown in RPMI-1640 (Invitrogen) and 10% (v/v) fetal bovine serum (FBS) (HyClone) at 37 °C and 5% CO_2. Cells were maintained at an average cell density of $\sim 2 \times 10^6$ cells mL^{-1}. U937 cells, derived from a human monocytic leukemia,[28] were grown in RPMI-1640 with L-glutamine (Invitrogen), 10% FBS (HyClone), and 1 mM sodium pyruvate (Sigma). Prior to measurement, MEL and U937 cells were washed twice in 1 × PBS and re-suspended in either 1 × PBS or 0.5 × PBS at a concentration of 3–5 × 10^5 cells mL^{-1}. This cell concentration range ensured that no more than one cell was present inside the pore at any given time.

Transit-time distribution modeling

We fit the τ-distributions derived from a single cell population with a log-normal distribution. For mixed cell populations that consist of two subpopulations and only one of which interacts specifically with a functionalized pore, we fit the τ-distributions with a mixture of two log-normals. The goodness of fitting is validated by the Kolmogorov–Smirnov (K–S) test. The p-values of the tests are calculated using simulations, since the critical region of the K–S test is no longer valid when the distribution parameters in the test are estimated from the data.[29] More details and illustrative examples are in ESI.†

As described in the Results and discussion section, we mixed MEL and U937 cells in ratios of 1 : 1, 1 : 3, and 1 : 9. For each of these mixed populations, we measured the transit time of cells as they pass through a blank pore, a pore functionalized with IgG2a (the control), and a pore functionalized with anti-CD34

antibody. Thus, we measured a total of 3 × 3 or 9 samples of cells from the 3 different mixture populations. In order to determine the mixture ratios, we used a unified constrained mixture model to fit the τ-distributions obtained when the mixed MEL and U937 cells traveled through the anti-CD34 antibody pore. We let $\boldsymbol{X}^{(i,j)}$ denote the transit time for the $1:3^{i-1}$ ($i = 1, 2, 3$) mixture of cells passing through the jth pore (1st pore: blank pore; 2nd pore: IgG2a pore; 3rd pore: anti-CD34 pore). Note that $\boldsymbol{X}^{(i,1)}$ and $\boldsymbol{X}^{(i,2)}$ were not fitted here due to the high similarity between MEL and U937 τ-distributions when these cells passed through a blank or non-specific pore (see Results and discussion section for details). We modeled the distribution of $\boldsymbol{X}^{(i,3)}$ ($i = 1, 2, 3$) by

$$f = a_1{}^{(i)} f_1{}^{(i)} + a_2{}^{(i)} f_2{}^{(i)}, \tag{3}$$

where a_1 and a_2 represent the mixture rates, and f_1 and f_2 are the two log-normal distributions with (mean, standard deviation) parameters denoted by ($\mu_1{}^{(i)}$, $\sigma_1{}^{(i)}$) and ($\mu_2{}^{(i)}$, $\sigma_2{}^{(i)}$), respectively. Each log-normal component corresponds to a subpopulation. We further placed the following constraints on the mixture model parameters ($\mu_1{}^{(i)}$, $\sigma_1{}^{(i)}$) and ($\mu_2{}^{(i)}$, $\sigma_2{}^{(i)}$):

$$\mu_1{}^{(i)} = \mu_1{}^{(i')} = \mu_1, \sigma_1{}^{(i)} = \sigma_1{}^{(i')} = \sigma_1 \text{ for any } i \neq i' \tag{4a}$$

$$\mu_2{}^{(i)} = \mu_2{}^{(i')} = \mu_2, \sigma_2{}^{(i)} = \sigma_2{}^{(i')} = \sigma_2 \text{ for any } i \neq i' \tag{4b}$$

These two constraints were based on the following considerations. The cell populations corresponding to $\boldsymbol{X}^{(i,3)}$ ($i = 1, 2, 3$) consist of the same type of subpopulations (MEL and U937 cells) passing through the anti-CD34 pore, which only specifically interacts with the MEL cells. The distributions of $\boldsymbol{X}^{(i,3)}$ ($i = 1, 2, 3$) are thus naturally expected to have the same mixture components (corresponding to the two cell subpopulations) but different mixture proportions. Eqn (3) was then simplified to

$$f = a_1{}^{(i)} f_1 + a_2{}^{(i)} f_2 \tag{5}$$

The optimal values for the distribution parameters can be derived by a Maximum Likelihood Estimation (MLE) approach[30] and an iterative expectation-maximum (EM) algorithm,[31] with two steps. The first is the *expectation step*: with initial guesses for the parameters of our mixture model, the "partial membership" of each data point in each constituent distribution is computed. That is, for each data point $x^{(i)}{}_m$ in the ith sample (corresponding to the cells with mixture rate $1:3^{i-1}$ passing through the 3rd pore) and the kth component distribution f_k, the membership value $y^{(i)}{}_{m,k}$ is:

$$y_{m,k}^{(i)} = \frac{\alpha_k^{(i)} f_k\left(x_m^{(i)}; \mu_k, \sigma_k\right)}{f\left(x_m^{(i)}\right)}, \tag{6}$$

where f denotes the mixture distribution in eqn (5).

The second step is the *maximum step*: with expectation values for group membership, the distribution parameters are recomputed. First, the mixing coefficients a_k's, the means of the membership values over all the data points, are recomputed by

$$\alpha_k^{(i)} = \frac{\sum_{m=1}^{n_{i3}} y_{m,k}^{(i)}}{n_{i3}} \tag{7}$$

where n_{i3} is the size of sample $\boldsymbol{X}^{(i,3)}$. The mixture component model parameters are then calculated using data points that have been weighted using the membership values,

$$\mu_k = \frac{\sum_{i=1}^{3}\sum_{m=1}^{n_{i3}} y_{m,k}^{(i)} x_m^{(i)}}{\sum_{i=1}^{3}\sum_{m=1}^{n_{i3}} y_{m,k}^{(i)}}, \sigma_k = \sqrt{\frac{\sum_{i=1}^{3}\sum_{m=1}^{n_{i3}} y_{m,k}^{(i)}\left(x_m^{(i)} - \mu_k\right)^2}{\sum_{i=1}^{3}\sum_{m=1}^{n_{i3}} y_{m,k}^{(i)}}} \tag{8}$$

The above model bears the following advantages: (1) the number of parameters is reduced compared to an unrestricted model and thus the estimation variances are smaller; and (2) there is less risk of an overfitting problem. The model constraints, naturally determined by the data property and experiment design, improve the reliability of the fitting.

Results and discussion

As proof-of-principle, we screened MEL cells based on the CD34 receptors expressed on their surface. A suspension of MEL cells was injected into (1) a blank pore; (2) a pore functionalized with rat IgG2a; and (3) a pore functionalized with anti-CD34 monoclonal antibody. Fig. 2a shows typical traces of the normalized current, $\delta I/I$, *vs.* time for cells passing through the three different pores: the pulses are well resolved in both magnitude and width. A distribution of size obtained when MEL cells flowed across a blank pore shows the variation within a single population of cells (Fig. 2b). A comparison among the different τ-distributions shows that MEL cells traveled slowest through the anti-CD34 pore. Further, as shown in Fig. 2c and d, the transit time significantly depends on the antibody concentration used to functionalize the pore. When the pores were functionalized with 100 μg mL^{-1} of antibody, the average transit time of MEL cells passing through an anti-CD34 pore was $\tau_{avg} = 7.35$ ms. This transit time was 1.21 ms and 0.67 ms longer than through the blank and the isotype-control pores, respectively. More importantly, when a 15-fold higher concentration of antibody, *i.e.* 1500 μg mL^{-1}, was used, τ_{avg} and the variance of the τ-distribution increased significantly only for the anti-CD34 pore (Fig. 2c and d). We attribute the increase in variance to the number of binding events that occur between cells with varying CD34 densities and the anti-CD34 pore. As described in the Materials and methods section, each distribution was fitted to a log-normal distribution (solid black curves).

As a further control of our ability to distinguish between specific and non-specific interactions, we flowed uniformly-sized SuperAvidin polystyrene colloids (9.95 ± 0.46 μm) conjugated with Streptavidin-labeled, anti-annexinV antibodies (at the saturation density of ~1.11×10^7 colloid^{-1}; see ESI) through a blank pore and one that had been functionalized with annexinV (50 μg mL^{-1}) (See ESI Fig. S5†). Similar to our observation with MEL cells, both the mean *and* the variance of the τ-distribution increased when specific protein–protein interactions occurred.

In Fig. 2e, we show $\delta\tau = (\tau_{avg} - \tau_{avg}{}^*)$, the difference in the mean transit time between the functionalized pore (τ_{avg}) and that of the blank pore ($\tau_{avg}{}^*$), *vs.* the antibody concentration, [*Ab*], used to functionalize the pore. Only the interaction between MEL cells and the functionalized anti-CD34 antibodies shows saturation.

As the concentration increases, the functionalized anti-CD34 antibody reaches maximum density, thus leading to a maximum number of protein–protein binding events possible. A slight increase in $\delta\tau$ is observed at low antibody concentrations for the isotype control. This surprising observation is most likely due to the fact that, at higher antibody densities, the surface charges collectively play a role in shielding the antibodies, thereby reducing non-specific interactions. Further work, however, is needed to confirm this. Nonetheless, despite the slight rise in average transit time at low concentrations of isotype-control antibody, the specific interaction between MEL cells and the functionalized anti-CD34 antibodies is clearly demonstrated.

The anti-CD34 pore data in Fig. 2e are described by $\frac{\delta\tau_{max}[Ab]}{K_\tau+[Ab]}$, where $\delta\tau_{max} = (\tau_{avg}-\tau_{avg}{}^*)_{max}$ and K_τ is the concentration of functionalized protein necessary to achieve a half-maximum transit-time increase. $\delta\tau_{max}$ and K_τ are both a function of the affinity between the protein receptor and functionalized protein and also the protein-receptor density at a given shear stress. For a CD34 receptor–anti-CD34 antibody pair and a shear stress of $\sim$330 dyn cm^{-2} near the pore walls, $\delta\tau_{max}$ = 4.78 ms and $K_\tau = 3.20 \times 10^2$ μg mL^{-1}. The specificity of $\delta\tau_{max}$ and K_τ shows that our assay could serve as a tool to study the interactions between proteins bound to substrates that are in relative motion to one another (in contrast to the case where they are free in solution and interact diffusively).

For proof-of-principle, we characterized a *single* population of cells that were all positive for one particular cell-surface marker; however, a more powerful demonstration would be to screen a *mixed* population in which only a subpopulation of cells are positive for a specific marker of interest. Therefore, we mixed two different types of cells—MEL and U937—in different proportions (1 : 1, 1 : 3, and 1 : 9) and subsequently screened the resulting mixtures with a pore functionalized with 500 μg mL^{-1} of anti-CD34 antibody. For control purposes, we also screened the same mixtures of cells with a blank pore and a pore functionalized with 500 μg mL^{-1} IgG2a isotype control antibody. If we compare the τ-distributions of a *single* population of MEL cells and U937 cells traveling in a blank pore (see Fig. S4 in the ESI†), we observe that the two distributions are shifted apart by $\sim$1 ms. This shift is most likely due to different cell properties (*i.e.* size, density, and stiffness),[32] although further experiments are needed to confirm this. Despite the transit-time shift, the two τ-distributions still overlap greatly. Figs. 3a–c show the τ-distributions (black histograms) obtained for the different mixtures, 1 : 1, 1 : 3, and 1 : 9 of MEL and U937 cells, respectively, when screened with the blank pore (left), the IgG2a antibody pore (middle), and the anti-CD34 antibody pore (right). From the figures, we first see that the left column (corresponding to cells passing through a blank pore) presents a distribution shift in increasing time from the top to the bottom, consistent with the fact that U937 cells travel slower than MEL cells in a blank pore (Fig. S4†) and the fact that the percentage of U937 cells increases from the top to the bottom in Fig. 3. More importantly, the left column figures also show that we are unable to distinguish between MEL and U937 cells when they transit the blank pore as a mixture. This agrees well with the observed large overlap of τ-distributions for single populations of MEL and U937 cells in Fig. S4. In the middle column of Fig. 3, where a mixed population of MEL and U937 cells transits a pore functionalized with an isotype control antibody, we make similar observations that the distributions for different types of cells look non-separable. This is expected since only non-specific interactions are present. In contrast, when a mixture of cells transit through an anti-CD34 antibody pore, only the MEL cells interact specifically with the functionalized anti-CD34 antibodies, thus increasing their transit time through the pore; the U937 cells are not affected, as these cells are human and therefore do not interact with the murine-specific monoclonal anti-CD34 antibody. The net result is that the overall τ-distribution is significantly broader than that obtained when the same mixture of cells passed through a blank or an IgG2a pore. This higher data spreadness, together with the observed separate distribution peaks, increases the promise of separating the distributions for different cell types.

Naturally, we consider fitting a mixture of two log-normal distributions to distinguish between the MEL and U937 cells and further to determine the mixture ratio. However, a direct individual fitting to each of the mixed populations is not favored due to the following considerations: (1) the sample sizes are quite different, which would result in different levels of confidence and risk of the fitted model, essentially, the results from small samples are much less trustworthy; and (2) individual fittings miss the fact that the mixed populations contain the same type of subpopulations though with different mixture rates. These considerations motivated our unified constrained mixture model (see Materials and methods section). With the "unified" property, our model allows a small sample to adjust its fitting by borrowing information from larger samples in addition to the possible information exchange among the large samples. With the "constrained" asset, our model reduces the parameter space reasonably and thus improves the reliability of the fitting.

Based on the unified constrained model, we fitted the distributions in the right column (anti-CD34 antibody pores) with a mixture of two log-normal distributions (identified as *1* and *2* in the figures) corresponding to the two different cell populations. The details of the model fitting were described in the Materials and methods section. Briefly, we conducted the fitting using a Maximum Likelihood approach[30] and an iterative expectation-maximum algorithm.[31] The ratio of the cells obtained from the unified constrained model is close to the actual mixture ratios. Differences between the two are most likely a result of error introduced when counting the cells with a hemocytometer during cell suspension preparation and other variations. Furthermore, the first mixture component, log-normal *1*, has a larger mean and variance as compared to the second component, log-normal *2*. This result correlates well with the case of a single MEL cell population traveling across an anti-CD34 pore and is likely due to varying CD34 densities on the MEL cell surface. For the bottom figure in the right column of Fig. 3, there is another noteworthy issue. In particular, the mixed cell population in that experiment is very small. With the 1 : 9 mixture rate, only 20 MEL cells were measured. This small size raised a serious over-fitting problem and led to an inaccurate estimation of the mixture rate when the data were fitted without using the unified constrained model. As a comparison, our model helped recover the mixture rate, though the fitting seemed poor. We would say this is a *preferred* "poor" fitting.

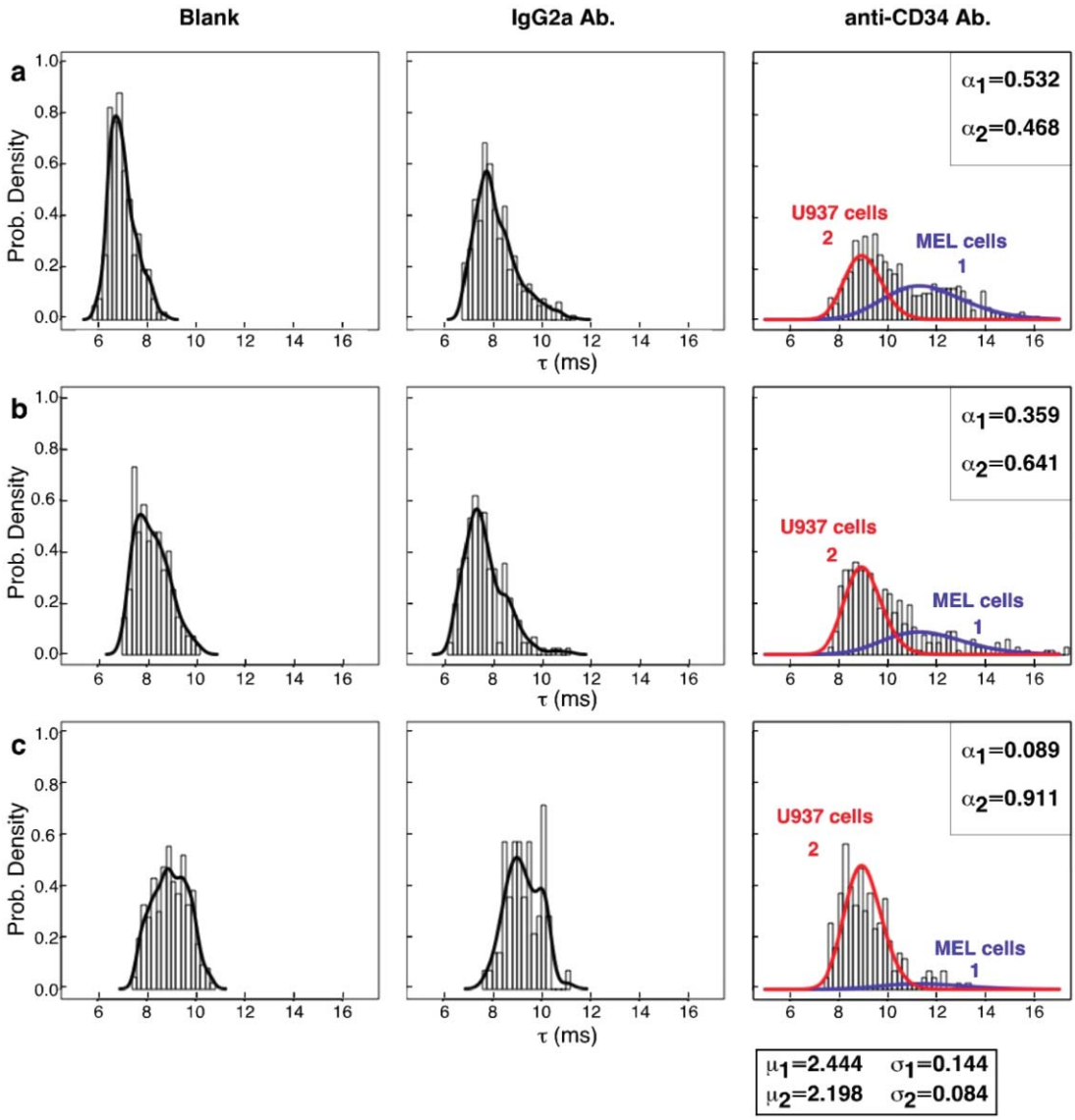

Fig. 3 Detection of MEL cells within a mixed cell population. τ-distributions and their fitting curves for mixtures with different proportions of MEL cells and U937 cells ($\sim 5 \times 10^5$ cells mL^{-1}) flowing (10.0 kPa) through a blank pore (left column), a pore functionalized with either IgG2a (middle column) or anti-CD34 antibody (right column). The antibody concentration for pores functionalized with IgG2a and anti-CD34 antibody was 500 μg mL^{-1}. Each distribution obtained (black histogram) when cells traveled through an anti-CD34 antibody pore was modeled with a mixture of two log-normal distributions (right column), identified as *1* and *2* in the figure. The distribution parameters were estimated through a unified constrained model. The parameters of the fittings (μ = mean and σ = standard deviation of the distribution calculated after taking the logarithm of the data) as well as the mixture ratios (α) are provided in the figure. MEL cells (blue distribution) traveled significantly slower than U937 cells (red distribution) in the anti-CD34 antibody pore due to specific interactions (right-most column). (a) The ratio of MEL to U937 cells was 1 : 1. The number of cells measured in the blank pore was 182 cells; in the IgG2a pore, 366 cells were measured; and in the anti-CD34 pore, 541 cells were measured. (b) The ratio of MEL to U937 cells was 1 : 3. The number of cells measured in the blank pore was 137 cells; in the IgG2a pore, 335 cells were measured; and in the anti-CD34 pore, 336 cells were measured. (c) The ratio of MEL to U937 cells was 1 : 9. The number of cells measured in the blank pore was 431 cells; in the IgG2a pore, 69 cells were measured; and in the anti-CD34 pore, 213 cells were measured.

The specific protein–protein interactions that occur in our protein-functionalized pores are observable in not only the cell transit time but also the shape of individual resistive pulses. When α in eqn (2) is constant, the pulse is flat (Fig. 4a, top). In contrast, when α periodically changes, as it does for a cell tumbling across the pore with period T, the pulse exhibits oscillations (Fig. 4a, bottom). We observed both types of pulses (Fig. 4b, top) when MEL cells passed through either a blank (Fig. 4b, middle) or an anti-CD34 (Fig. 4b, bottom) pore. As shown in Fig. 4c, the observed period of oscillation in a blank pore (red) is always less than that in an anti-CD34 pore (green), reflecting the fact that CD34 receptors transiently bind to the functionalized anti-CD34 antibodies and subsequently retard the cell's motion. Although further studies are needed, a cell's transit time combined with an analysis of its pulse shape could ultimately provide *quantitative* information regarding the density of a specific receptor on that cell's surface.

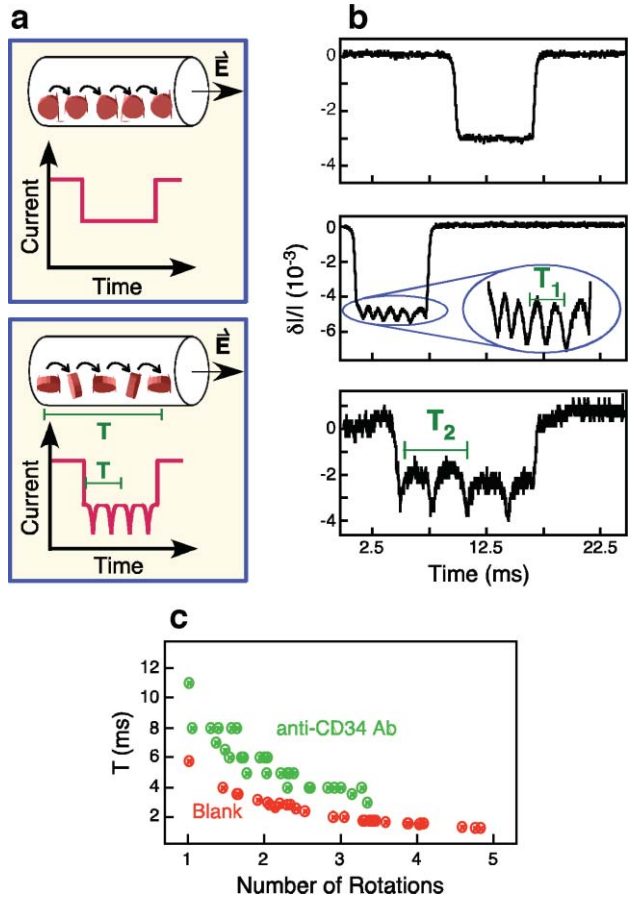

Fig. 4 Pulse-shape analysis. (a) Effect of cell orientation on pulse shape. Flat resistive pulses occur when the orientation of the cell remains constant with respect to the electric field $\vec{E}$ parallel to the pore's central axis (top). In contrast, pulses show oscillations due to the different orientations of the cell with respect to $\vec{E}$ as it flows across the pore (bottom). T corresponds to the period of one complete cell revolution. (b) Examples of different pulse shapes obtained when MEL cells flowed through a blank and a functionalized anti-CD34 pore: a flat pulse (top); a pulse that oscillates with period T_1 in a blank pore (middle); and a pulse that oscillates with period T_2 in a functionalized pore (bottom). (c) T *vs.* number of rotations in a blank pore (red) and in a pore functionalized with anti-CD34 antibody (green).

The exquisite sensitivity and simplicity of our pore method imparts a number of general advantages over other current cell characterization methods. First, exogenous labeling is not required. This significantly reduces both cost and sample preparation time and is especially attractive in cases where it is not known whether labeling affects cell physiology and function. Second, accuracy is not lost as a result of the small number of cells interrogated. Thus, our method is suitable for cases in which only a few hundred cells are available for interrogation. Third, separation (using microfluidic valves) and recovery of cells for further propagation are possible.

In this initial work, we have demonstrated only proof-of-principle of our ability to use a functionalized pore to characterize cells. Although we have chosen to perform all our measurements using a pore whose size is 800 μm × 15 μm × 15 μm (L × W × H), our signal-to-noise ratio (based largely on $\delta I/I \sim V_{cell}/V_{pore}$) is such that we could employ pores with much larger cross-sectional area (*e.g.* greater than 25 μm × 25 μm) and, correspondingly, shorter length to accommodate a mixture of cells whose components range in size from 5 μm to beyond 25 μm. The non-pulsatile flow rate of 10.0 kPa is the lower limit of the microfluidic pump employed. As mentioned in the Materials and methods section, a flow rate as high as 34.0 kPa has been used with no detectable loss in pulse-width (or height) resolution. Further studies, however, are needed to identify the upper-limit flow rate to detect specific interactions between ligand and receptor with a specific affinity. That our data acquisition provides a time resolution of 20 μs strongly suggests that there is sufficient flexibility in pore design.

We envision that, with minor modifications to our microfluidic device, *i.e.* placing a blank, a control, and a specifically-functionalized pore in series, single-cell analysis based on surface receptors can be realized. Similarly, full-phenotypic characterization of cells can be achieved, as a "decision tree" of multiple pores, each linked sequentially to one another and each functionalized with a different protein corresponding to a difference cell-surface marker, can easily be created. Although the throughput of a single pore is not comparable to that of flow cytometry (100's cells min^{-1} *vs.* 10 000 cells s^{-1}), our microfluidic platform enables the construction of arrays of pores[24] for performing many measurements or assays in parallel. Finally, our measurements are sensitive to the density of receptors on the cell surface. For those cells that express low levels of receptors on the cell surface, the flow rate in our pore could be readily reduced to increase sensitivity.

Conclusions

In conclusion, we have demonstrated a label-free, highly-sensitive, and accurate method for characterizing cells based on their cell-surface components. The generality of our method—the pore functionalization is not specific for one particular antigen/antibody complex—and the simplicity of approach are such that it could be extended to perform different types of *in vitro* cell-based assays, such as assessing apoptosis and cell viability. Furthermore, it could be used for such specific applications as investigating cell-surface receptor densities during stem-cell differentiation.[33]

Acknowledgements

The authors thank J. Crispino and A. Fischer for providing MEL and U937 cells, respectively; A. Fischer for help with cell culturing; H. Nolla for assistance with flow cytometry; and S. E. Ruzin and A. Radenovic for help with the wide-field deconvolution microscopy. The authors also thank O. A. Saleh, J. Auger, R. Duggan, A. Radenovic, and D. J. Beebe for critical reading of this manuscript.

This work has been partially supported by NIEHS Grant No. 2 P42 ES004705-19 and NSF Grant No. CBET-0651799.

References

1 P. J. L. Lane, F. M. C. Gaspal, and M. Y. Kim, *Nat. Rev. Immunol.*, 2005, **5**, 655–660.

2 C. Kemper and J. P. Atkinson, *Nat. Rev. Immunol.*, 2007, **7**, 9–18.
3 O. Hrusak and A. Porwit-MacDonald, *Leukemia*, 2002, **16**(7), 1233–1258.
4 D. Lau, L. Guo, R. Liu, J. Marik and K. Lam, *Lung Cancer*, 2006, **52**(3), 291–297.
5 V. J. Hruby, *Nat. Rev. Drug Discovery*, 2002, **1**, 847–858.
6 H. M. Shapiro, in *Practical Flow Cytometry*, 4th edn, Wiley, 2003.
7 W. Denk, J. H. Strickler and W. W. Webb, *Science*, 1990, **248**(4951), 73–76.
8 P. Lang, M. Pfeiffer, R. Handgretinger, M. Schumm, B. Demirdelen, S. Stanojevic, Th. Klingebiel, U. Köhl, S. Kuci and D. Niethammer, *Bone Marrow Transplant.*, 2002, **29**(2), 497–502.
9 K. Wang, M. K. Marshall, G. Garza and D. Pappas, *Anal. Chem.*, 2008, **80**, 2118–2124.
10 K. Cheung, S. Gawad and P. Renaud, *Cytometry, Part A*, 2005, **65**, 124–132.
11 O. A. Saleh and L. L. Sohn, *Rev. Sci. Instrum.*, 2001, **72**(12), 4449–4451.
12 W. H. Coulter, US Pat. 2,656,508, 1953.
13 R. W. Deblois and C. P. Bean, *Rev. Sci. Instrum.*, 1970, **41**(7), 909–916.
14 X. Cheng, D. Irimia, M. Dixon, K. Sekine, U. Demirci, L. Zamir, R. G. Tompkins, W. Rodriguez and M. Toner, *Lab Chip*, 2007, **7**, 170–178.
15 S. E. Weigum, P. N. Floriano, N. Christodoulides and J. T. McDevitt, *Lab Chip*, 2007, **7**, 995–1003.
16 Y. N. Xia and G. M. Whitesides, *Angew. Chem. Int. Ed.*, 1998, **37**, 551–575.
17 S. Karrasch, M. Dolder, F. Schabert, J. Ramsden and A. Engel, *Biophys. J.*, 1993, **65**, 2437–2446.
18 J. L. Wilbur, A. Kumar, H. A. Biebuyck, E. Kim and G. M. Whitesides, *Nanotechnology*, 1996, **7**(4), 452–457.
19 K. D. Patel, M. U. Nollert and R. P. McEver, *J. Cell Biol.*, 1995, **131**(6(2)), 1893–1902.
20 R. J. Galloway, Seradyn, Inc., Indianapolis, IN, 1988.
21 C. Cozens-Roberts, J. A. Quinn and D. A. Lauffenberger, *Biophys. J.*, 1990, **58**, 107–125.
22 J. Clausen, in *Laboratory Techniques in Biochemistry and Molecular Biology, Vol. 1*, ed. T. S. Work and N. Work, North-Holland Publishing Co., New York, 1981.
23 O. A. Saleh and L. L. Sohn, *Proc. Natl. Acad. Sci. U. S. A.*, 2003, **100**(3), 820–824.
24 A. Carbonaro and L. L. Sohn, *Lab Chip*, 2005, **5**(10), 1155–1160.
25 R. W. Deblois, C. P. Bean and R. K. A. Wesley, *J. Colloid Interface Sci.*, 1977, **61**, 323–335.
26 D. C. Golibersuch, *J. Appl. Phys.*, 1973, **44**(6), 2580–2584.
27 D. C. Golibersuch, *Biophys. J.*, 1973, **13**, 265–280.
28 D. L. Simmons, A. B. Satterthwaite, D. G. Tenen and B. Seed, *J. Immunol.*, 1992, **148**(1), 267–271.
29 M. A. Stephens, *J. Am. Stat. Assoc.*, 1974, **69**, 730–737.
30 M. S. Kay, in *Fundamentals of Statistical Signal Processing: Estimation Theory*, Prentice Hall, 1993, ch. 7.
31 P. K. MacKeown, in *Stochastic Simulation in Physics*, Springer, 1997.
32 M. J. Rosenbluth, W. A. Lam and D. A. Fletcher, *Lab Chip*, 2008, **8**, 1062.
33 S. K. Mohanty, M. J. Conboy, L. L. Sohn and I. Conboy, *unpublished work*.